mmWave/THz Reconfigurable Ultra-Wideband (UWB) Microstrip Antenna

Uri Nissanov* and Ghanshyam Singh

Abstract—The concept of ultra-wideband (UWB) reconfigurable mmWave/THz microstrip antenna with a newfangled gold radiating patch with two PIN diodes installed on a benzocyclobutene (BCB) polymer is presented. The reconfigurable types of the proposed antenna are frequencies, bandwidths (BWs), and beams reconfigurations. This reconfigurable antenna was designed and simulated with the time-domain based on a FIT solver at the CST MWS simulator, while the comparison was with the frequency-domain based on the FEM solver at the CST MWS simulator. The simulation results obtained from both solvers were in a fair agreement, supporting the proposed antenna design. These antennas may be used in cellular communication at mmWave/THz band for beyond 5G.

1. INTRODUCTION

Following [1–4], the millimeter-wave (mmWave) is a frequency band that ranges from 30 to 300 GHz, where the terahertz (THz) regime is a frequency band that ranges from 300 to 3000 GHz, within the millimeter-wave (mmWave) and optical bands, while other researchers define the THz band from the frequency of 100–10,000 GHz. The THz regime has not been studied in depth by scientists, owing to the deficiency of electronic power sources with power over ten dBm, power detectors, and high-gain antennas in this band. The outcome of high-frequency characteristics is a large absorption loss and is one of the main problems, so we need to use the frequency window in this regime, in which the absorption loss is below 10 dB/100 m. For example, the frequencies range between 125 and 175 GHz, approximately, have the absorption loss of 3 dB/100 m, with a worst-case scenario of rains at rates of 50 mm/h [5].

As the 5th generation (5G) communication networks are now putting into commercialization, technologies for the next-generation communications (i.e., 6G) are also being explored to achieve faster and more reliable data transmissions. Among these technologies, beam-steering, ultra-massive multi-input-multi-output (UM-MIMO), and reconfigurable microstrip antenna have received much interest.

Communication at THz bands has drawn antenna researchers' attention significantly since graphene ascends as an antenna design material. The graphene capability to sustenance surface plasmon polaritons (SPPs) modes at THz frequencies makes it possible to scale-down various communication types of equipment for sensing and communication systems. The antenna design using graphene [6–9] provides good matching, good total efficiency, impressive reconfiguration capabilities, and high miniaturization.

THz reconfigurable antennas show a solution that integrates numerous radios into an integrated circuit (IC). The integration of numerous radiation elements with reconfigurable antennas has become an essential feature of newfangled radio-frequency (RF) systems for the THz cellular communication, imaging, sensing, and satellite communications. There is a need to integrate RF, cognitive, and smart

devices, sensing the RF surrounding and communicating simultaneously in any dense environment. These capabilities include cognitive radios (CRs), solver-defined radios (SDRs), and frequency agile to manage the multiband operation and reconfigurable operation with adequate power and spectrum management. The competence of reconfigurable antennas to alter their functionality on requiring allows them to change the operating frequency, the bandwidth (BW), the main beam lobe direction, and polarization or a combination of them. Such antennas can avoid noise sources, provide broader coverage by steering the main lobe's angle, and improve the beam steering capability. These concepts may diminish the hardware intricacy, cost, and number of components to contemporary radio technology supported on communications systems without flexible hardware [10, 11].

In Reference [12], the researchers proposed two reconfigurable THz Vivaldi antennas founded on a hybrid metal-graphene formation for an operating frequency range 210–670 GHz metal-graphene Vivaldi antenna at a resonance frequency of approximately 300 GHz, and 1200 GHz for the graphene Vivaldi antenna. The reconfiguration was performed by changing the electrical field bias of the graphene layer. The modeling and simulation were performed with the computer simulation technology microwave studio (CST MWS) solver. The graphene-metal Vivaldi antenna's simulation results and the maximum gain and operating frequency of graphene Vivaldi antenna were as follows: 7 dB, 210–670 GHz and < 1 dB, 280–1400 GHz, respectively. In Reference [13], the researchers proposed a hybrid structure dielectric resonator antenna (DRA) paired with dipole graphene plasmon for the resonance frequency of 2500 GHz. The reconfiguration was performed by altering the electrical field bias of the graphene layer. The complex effective index and typical electric field index of the 2D pattern were found and simulated with the COMOSOL solver. The modeling and simulation of the antenna were performed with a CST MWS solver. The simulation results for maximum gain and radiation efficiency were found as 7 dB and 70%, respectively. In Reference [14], the researchers proposed a reconfigurable THz patch antenna using a graphene cavity for dual frequency bands of 4–5 THz and 6.5–7.5 THz. The suggested patch antenna was based on the backing cavity defined with interleaved graphene/Al_2O_3 stacks. The reconfiguration was carried out by changing the graphene layer electrical field bias. The modeling and simulation of the antenna were performed with a CST MWS solver. The maximum directivity, BW, and main lobe direction simulation results were 7.2 dBi, 1000 GHz, $-15°$ to $25°$, respectively. In Reference [15], the researchers proposed a 15×15 reconfigurable reflectarray (RRA) antenna at a resonance frequency of 220 GHz and based on a simple patch element. A PIN diode carried out the reconfigurable ability. The modeling and simulation of the antenna were performed with the Ansys high frequency structure simulator (HFSS) solver. The simulation results of the maximum directivity, beam scanning range, and aperture efficiency were: 21 dBi, $0°$–$50°$, and 43.7%, respectively. In Reference [16], the researchers proposed a two miniaturized dual-band graphene antenna array based on a photonic bandgap (PBG) dielectric laminate in the operating frequency band 850–1040 GHz. The reconfiguration was carried out by changing the electrical field bias of the graphene layer. The designed antennas were simulated and optimized by the CST MWS solver. The maximum gain, directivity, BW, and radiation efficiency achieved for the homogenous graphene and PBG graphene were 15.89 dB, 16.8 dBi, 28.13 GHz, 87%, 16.4 dB, 17 dBi, 33.34 GHz, and 86.67%, respectively. In Reference [17], the researchers proposed a two-element pattern reconfigurable patch antenna at a frequency of 0.6 THz. Two PIN diodes performed the reconfigurable capability. The modeling and simulation of the antenna were performed with the CST MWS solver. The simulation results of the maximum gain, directivity, BW, central lobe directions angles, and radiation efficiency were: 6.99 dB, 7.1 dBi, 54.66 GHz, $-26°$, $26°$, and 97%, respectively. In Reference [18], the researchers proposed a three-structure reconfigurable graphene antenna at a resonance frequency of 1780 GHz. The antenna model included a radiator graphene patch and a non-radiator graphene ring. The reconfiguration was carried out by changing the electrical field bias of the graphene layer. The design and simulation of the antenna were performed with the CST MWS solver. The simulation results of the maximum directivity and central lobe direction angles for antennas were: ≈ 5.8 dBi, $-30°$, and $-70°$, respectively. In Reference [19], the researchers proposed a beam reconfigurable quasi-Yagi-Uda microstrip antenna operating at 495–510 GHz, while the resonance frequency was around 500 GHz. On a metal-backed SiO_2 substrate, the antenna consists of a copper microstrip transmission line, a copper reflector, a copper half-round microstrip patch, and three groups of monolayer-graphene-patch directors. The reconfiguration was performed by changing the electrical field bias of the graphene layer. The modeling and simulation of the antenna were performed with

the Ansys HFSS solver. The simulation results of the maximum gain, BW, radiation efficiency, and central lobe direction angles were: 7.5 dB, 15 GHz, 96%, and 30–150°, respectively. In Reference [20], the researchers proposed a BW reconfiguration established on a concentric slot torus antenna using graphene, while the resonance frequency was between 4854 and 4878 GHz, and the working frequency was between 4667 and 5073 GHz. The reconfiguration was carried out by changing the electrical field bias of the graphene layer. The modeling and simulation of the antenna were performed with the CST MWS solver. The simulation results of maximum gain and BW were: 8.6 dB and 255–406 GHz, respectively. In Reference [21], the researchers proposed a reconfigurable graphene-based metal planar microstrip antenna, while the resonance frequency was between 990 and 1240 GHz, and the working frequency was between 700 and 1505 GHz. The reconfiguration was carried out by changing the electrical field bias of the graphene layer. The modeling and simulation of the antenna were done with the Ansys HFSS solver. The simulation results of maximum radiation efficiency and BW were: 69% and ≈ 805 GHz, respectively.

This research studies the design and simulation of an ultra-wideband (UWB) reconfigurable microstrip antenna for the frequency range of 100–302.85 GHz for beyond 5G wireless communication at the mmWave/THz band. Moreover, this antenna includes two PIN diodes. This paper is organized as follows. Section 1 exhibits the introduction and the related works. Section 2 shows the proposed antenna design and analysis. Section 3 shows the simulation and comparison results and discussion. Finally, Section 4 concludes this work.

This research paper's novelty is to design a mmWave/THz band UWB reconfigurable microstrip antenna with a novel gold radiating element mounted on a benzocyclobutene (BCB) polymer. This reconfigurable microstrip antenna was frequency, BW, and beam reconfiguration types. The design was carried out with the time-domain solver at the CST MWS simulator, while the comparison was carried out with the frequency-domain solver at the CST MWS simulator.

2. PROPOSED ANTENNA DESIGN AND ANALYSIS

A UWB reconfigurable microstrip antenna with a novel patch for the frequency range of 100–302.85 GHz was modeled and simulated in this study.

2.1. Introduction of Reconfigurable Microstrip Antenna

Following [10, 11, 22], wireless communications systems' rapid growth is limited because the electromagnetic (EM) spectrum has become overcrowded. THz cellular communications need to be reconfigurable to solve this challenge. They will have the capacity and intelligence to support the best suitable communications master plan based on signal quality evaluation and channel sensing activities.

Reconfigurable antennas can be sorted into four different types [10, 11, 22] (a) Frequency reconfigurable antenna: a radiator can alter its working frequency by leaping through diverse frequency bands. (b) Pattern reconfigurable antenna: the radiating structure can tune its radiation pattern. In this type, the antenna radiation pattern alters in terms of gain, direction, or shape. (c) Polarization reconfigurable antenna: a radiator can change its polarization, such as vertical/horizontal, righthand, or left-hand circular polarized (RHCP, LHCP). (d) This category is an integration of the last three categories. Reconfigurable antennas with adaptive radiation features must achieve these flexibilities in place of conventional antennas, whose formations are matched to specific specifications. A reconfigurable antenna can also be used to enhance security, refrain interference, and facilitate signal quality decline caused by multi-path fading by using cognitive radio communications and UM-MIMO techniques. Four significant reconfiguration types are used to implement reconfigurable antennas. (a) Antennas are based on switching out or in parts of the antenna structure with switches such as PIN diodes, varactor diodes, and RF microelectromechanical systems (MEMS) to alter their surface currents, which are defined as electrically reconfigurable. (b) Antennas using photoconductive switching elements are called optically reconfigurable antennas. (c) Physically reconfigurable antennas can be obtained by altering the geometry of the antenna. (d) Reconfigurable antennas can be applied via the exploit of smart materials, in which the characteristics of the substrate antenna can be changed, such as ferrites and liquid crystals.

2.2. PIN Diode Fundamentals

Following [23, 24], the PIN diode is a current-controlled resistor at microwave and RF signal. A silicon semiconductor diode, in between an N-type and a P-type region, is a high intrinsic I-region. The resistance of the PIN diode is set only by the forward-biased direct current (DC). The PIN diode can control the attenuator's RF signal level without introducing distortion, changing the RF signal's shape. An essential character of the PIN diode is its capability to control large RF signals when exceedingly smaller DC excitation level is used. PIN diode switches are often chosen as excellent mmWave switches for their high power handling capability and high third-order intercept point (IP3), as well as their high cutoff frequencies (up to 1500 GHz). A PIN diode, used as a switch, has two coequal states: OFF and ON states [24]. The ON state is frequently represented by a parasitic inductor L, which is usually below 150 pH (pH $= 10^{-12}$ H), in series with a low ohmic resistor R, having a resistance of about 10 Ω, while the OFF state is represented by a parasitic capacitor C, which is generally less than 50 f (fF $= 10^{-15}$ F), in series with the same parasitic inductor L, as the ON states.

3. THE FORMATION OF THE DESIGNED PROPOSED RECONFIGURABLE MICROSTRIP ANTENNA

This antenna included a novel gold radiation element and was made with BCB polymer from the Cyclotene series 3000 as a dielectric substrate for the microstrip antenna with the parameters of substrate height (h), gold thickness (t), dielectric constant (ε_r), and loss tangent ($\tan\delta$) of 30 μm, 2 μm, 2.6, 0.009 @65 GHz, respectively. The simulation results would be closest to the simulation for the frequency range of 100–302.85 GHz, because $\tan\delta$ and ε_r were taken upon the BCB polymer measurements, which was done [25] at the highest frequency, 65 GHz. One of the most critical BCB polymer features is the small $\tan\delta$ value, which assures low losses. The frequency behavior of both $\tan\delta$ and ε_r is almost constant below 1500 GHz [25]. Furthermore, this polymer's ε_r is almost constant
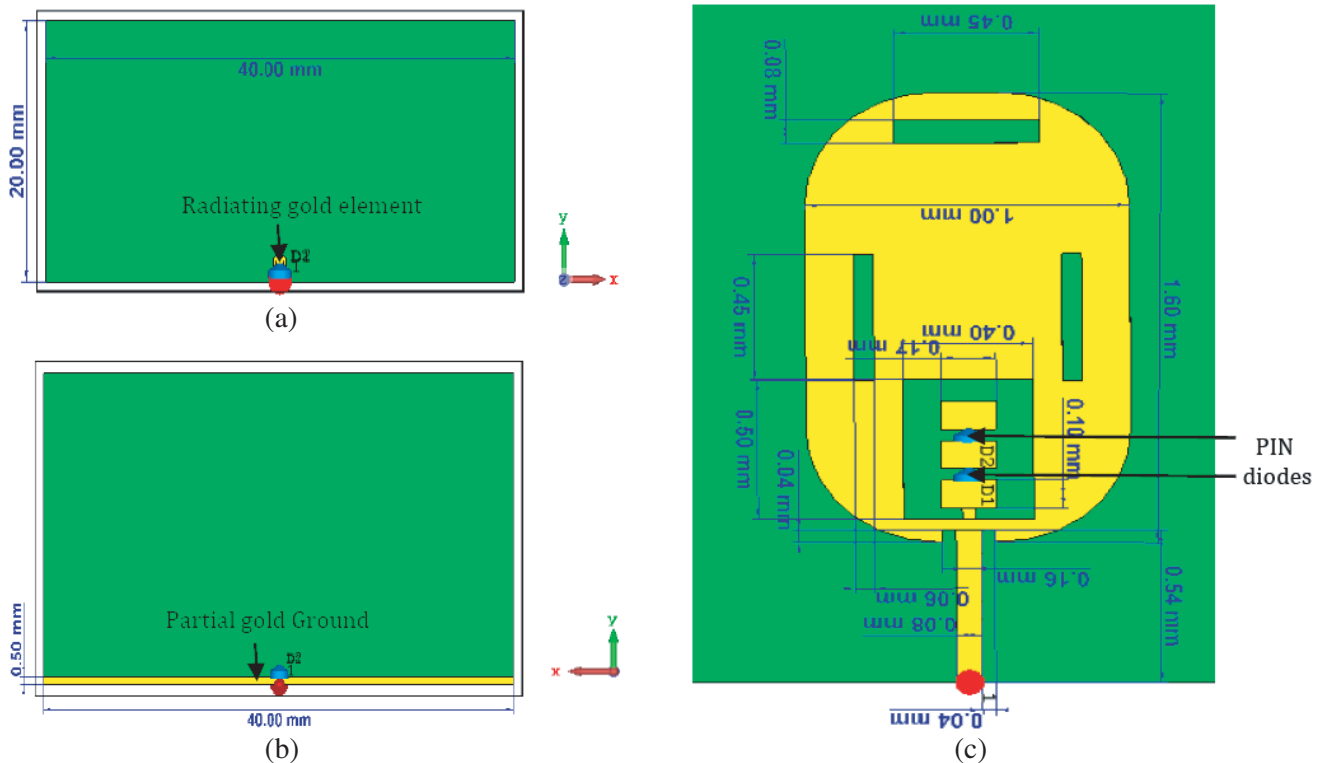

Figure 1. Structure of the proposed reconfigurable microstrip antenna. (a) Front view. (b) Back view. (c) Zoomed view of the radiating element.

under ambient temperature change up to $150°C$ [26–28]. All conductors were made of lossy metal of gold, and the electric conductivity of the lossy gold was applied as $4.561 \cdot 10^7$ S/m at the CST MWS simulator, while the lossy metal of gold model was also applied at the CST MWS simulator.

This substrate is electrically extremely ultrathin ($h = 30\,\mu m \leq \lambda_0/4$), for the sake of suppressing the surface wave in the THz band. This antenna includes 2 PIN diodes (D1, D2) as switches. The following figure (Fig. 1) is attached.

Figure 1 describes the structure of the designed reconfigurable microstrip antenna. All of the radiating elements' dimensions and partial ground sizes were optimized with the parameter sweep at the CST MWS solver. The dimensions of the substrate were $(40 \times 20)\,\text{mm}^2$. The PIN diodes (D1 and D2) were simulated as lumped elements (R, L, and C) according to the PIN diode electrical equivalent models at ON and at OFF states [24], when the optimal values of R, L, and C of the PIN diodes were set, according to the parameter sweep at the CST MWS solver as $10\,\Omega$, $100\,\text{pH}$ and $4\,\text{fF}$, respectively.

4. SIMULATION & COMPARISON RESULTS AND DISCUSSION

There are two accepted ways of validating the design and simulation results [29]: experimental verification and simulator verification/comparison. In this paper, the simulator verification/comparison was chosen.

The three-dimension (3D) commercial EM CST MWS simulator contains different solvers in which each solver works with different techniques [30]. The CST MWS has the time-domain solver based on the finite integration technique (FIT) describing Maxwell's equations in a time-grid space. The CST MWS simulator also has a frequency-domain solver, whereas this solver is based on the finite element method (FEM).

This paper's design and simulation were carried out with the FIT solver at the CST MWS simulator (2020 version). Comparing the designed and simulation results of the proposed reconfigurable microstrip antenna was carried out with the FEM solver at the CST MWS simulator.

Printed circuit board (PCB) technology requirements for mmWave interconnect and the antenna are very tight, and the minimum fabrication etching can be around $40\,\mu m$. In comparison, the declared etching accuracy is about $\pm 5\,\mu m$ [31], so in this research, the minimum etching was taken as $40\,\mu m$. To show the possible errors of this future fabrication, simulations were also performed on the possibility of this accuracy, i.e., for each dimension of the antenna that has been optimized, the possible production accuracy was added/subtracted in the simulation software, and two more simulations were performed with the new values that can be after the production of the proposed antenna. Therefore, two more graphs were obtained for S_{11} which may show the S_{11} that can be obtained in prototype fabricated antenna.

The PIN diodes (D1 and D2) were simulated as a lumped element (R, L, and C), according to the PIN diode electrical equivalent models at ON and OFF states [24], and the different modes are summarized at the following Table 1.

Table 1. The different modes of the proposed reconfigurable microstrip antenna.

Mode	PIN diode D1 state	PIN diode D2 state
mode 1	OFF	OFF
mode 2	OFF	ON
mode 3	ON	OFF
mode 4	ON	ON

According to the two PIN diodes states, Table 1 shows the different modes of the designed reconfigurable microstrip antenna.

4.1. Simulation Results of the Proposed Reconfigurable Microstrip Antenna at Modes 1–4

The next simulation results are shown in Figs. 2–8.
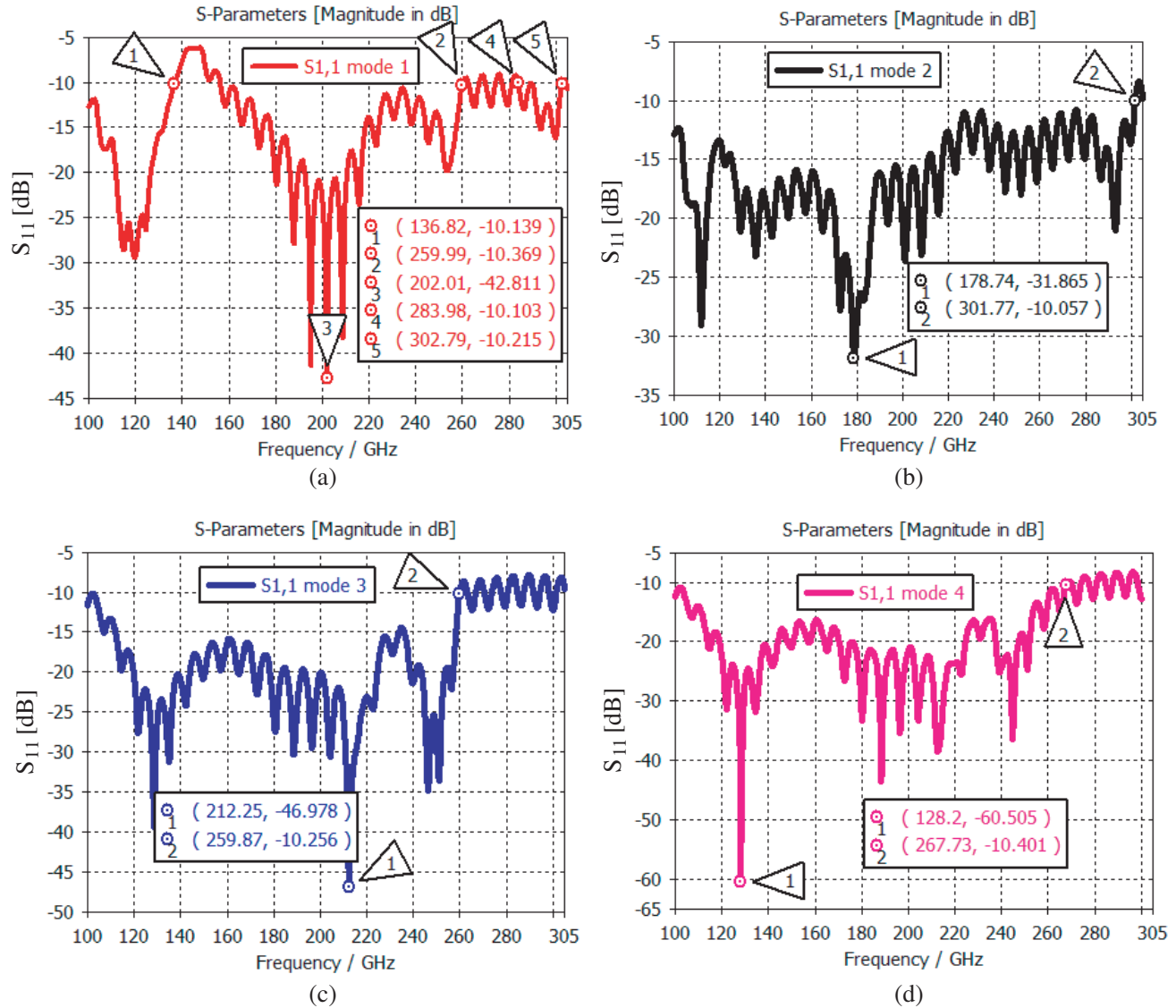
Figure 2. Simulation results of the return loss (S_{11}) for the proposed reconfigurable microstrip antenna. (a) For mode 1. (b) For mode 2. (c) For mode 3. (d) For mode 4.

Figures 2(a)–(d) show the simulation result of return loss (S_{11}) in (dB) of the proposed reconfigurable microstrip antenna at modes 1–4. It has been shown that the BWs of this antenna in modes 1–4 are: BW $(S_{11} \leq -10\,\text{dB}) > 159.98$ GHz$(>80.54\%)$, BW $(S_{11} \leq -10\,\text{dB}) > 201.77$ GHz $(>100.44\%)$, BW $(S_{11} \leq -10\,\text{dB}) > 159.96$ GHz $(>88.88\%)$, BW $(S_{11} \leq -10\,\text{dB}) > 168.05$ GHz$(>91.31\%)$, respectively. Furthermore, the resonance frequencies (f_0) at modes 1–4 are: 202 GHz, 178.74 GHz, 212.25 GHz, 128.2 GHz, respectively.

Figures 3(a)–(d) show the simulation result of the gain (IEEE) in (dB) of the proposed reconfigurable antenna at modes 1–4 while Phi $= 44°$. It has been shown that the gains for modes 1–4 are 0.93–8 dB, 0.28–8.47 dB, 0.42–8.46 dB, 0.2–8.59 dB for the frequency range of 100–300 GHz,
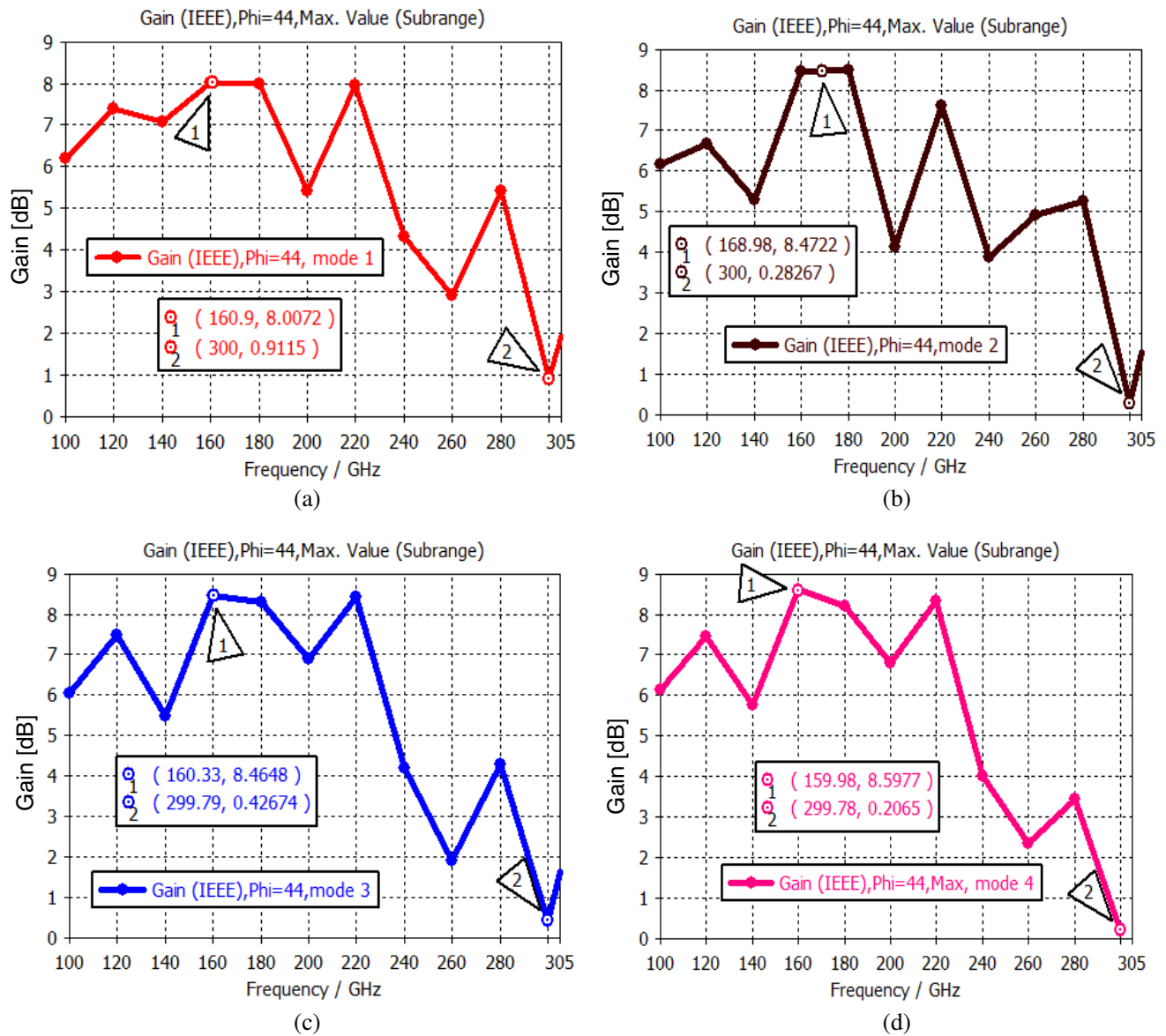
Figure 3. Simulation results of the gain for the proposed reconfigurable microstrip antenna. (a) For mode 1. (b) For mode 2. (c) For mode 3. (d) For mode 4.

respectively.

Figures 4(a)–(d) show the simulation results of the directivity in (dBi) at 3D result of the proposed reconfigurable antenna (modes 1–4) @160 GHz. It has been shown that the directivities at modes 1–4 were found as 8.32 dBi, 8.82 dBi, 8.76 dBi, 8.9 dBi @160 GHz, respectively.

Figures 5(a)–(d) show the simulation result of the proposed reconfigurable antenna's radiation and total efficiency (modes 1–4). It has been shown that radiation efficiency and total efficiencies of the proposed reconfigurable antenna at modes 1–4 are 78.13–94.42%, 70.92–93.4%, 67.9–89.1%, 78.2–93.17%, 77.85–93.85%, and 73.67–92.96% at the frequency range of 100–300 GHz, respectively.

Figures 6(a)–(d) show the comparison between the simulation results of the E-field in (dB) at the frequencies of 100 GHz, 180 GHz, and 300 GHz of the proposed reconfigurable antenna (modes 1–4). It has been shown that the E-field of the proposed reconfigurable antenna is −0.46–(6.1) dB at these frequencies. Furthermore, vit has been shown that the main lobes' angles are: −90, 77, 90, 96, 97, and 103° when these angles depend on the PIN diodes states.
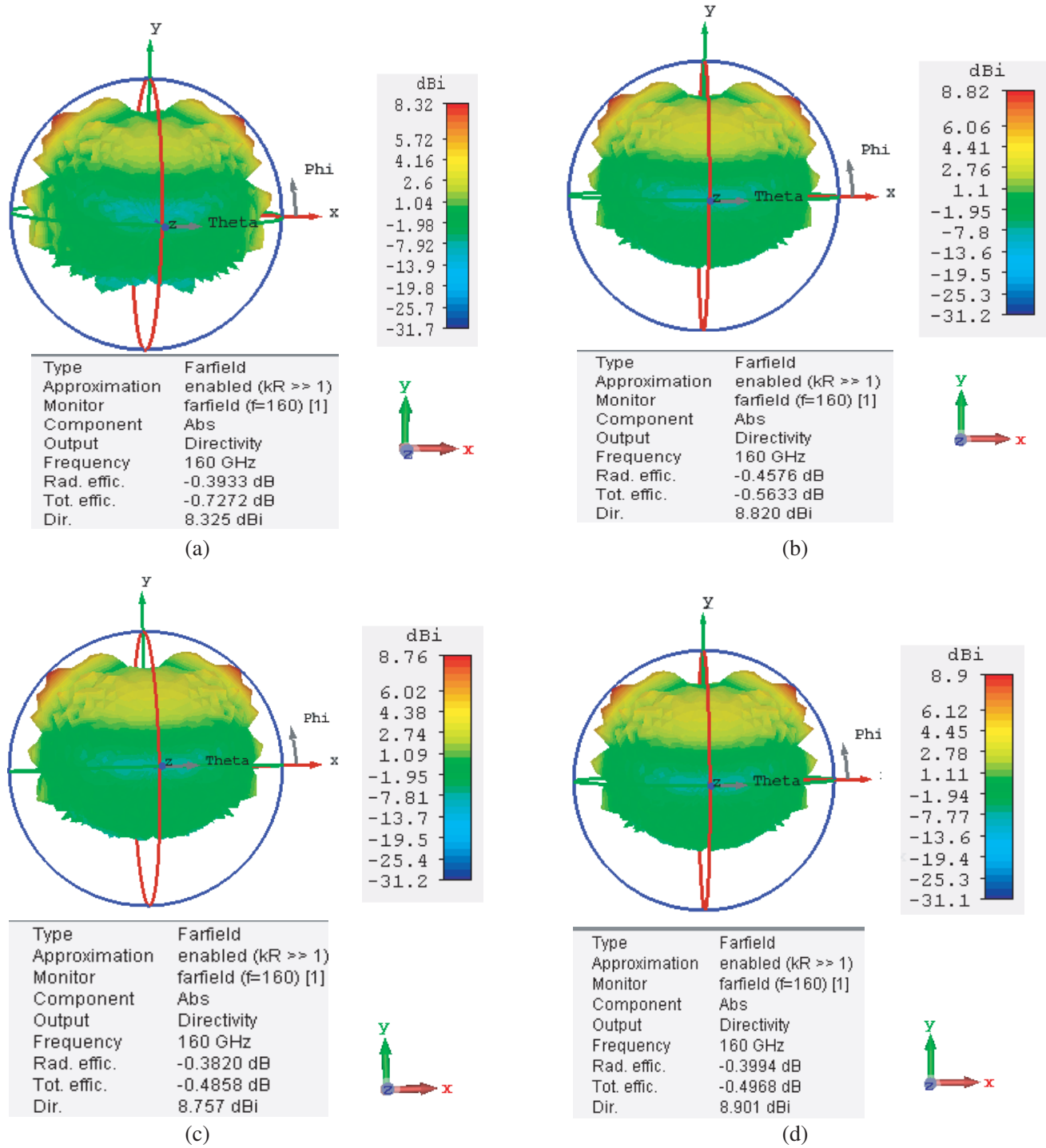
Figure 4. Simulation results of the directivity at the 3D result of the proposed reconfigurable microstrip antenna. (a) For mode 1. (b) For mode 2. (c) For mode 3. (d) For mode 4.

Figures 7(a)–(h) show the simulation results from a comparison of the surface current distribution at the (dB max A/m) at the frequencies of 100 GHz and 300 GHz of the proposed reconfigurable antenna at modes 1–4. It has been shown that the surface current distribution of the proposed reconfigurable antenna is between 1367 and 1531 A/m at the frequencies of 100 GHz and 300 GHz. It is also shown that the surface current distribution is concentrated at the edges of the gold patch. Moreover, at
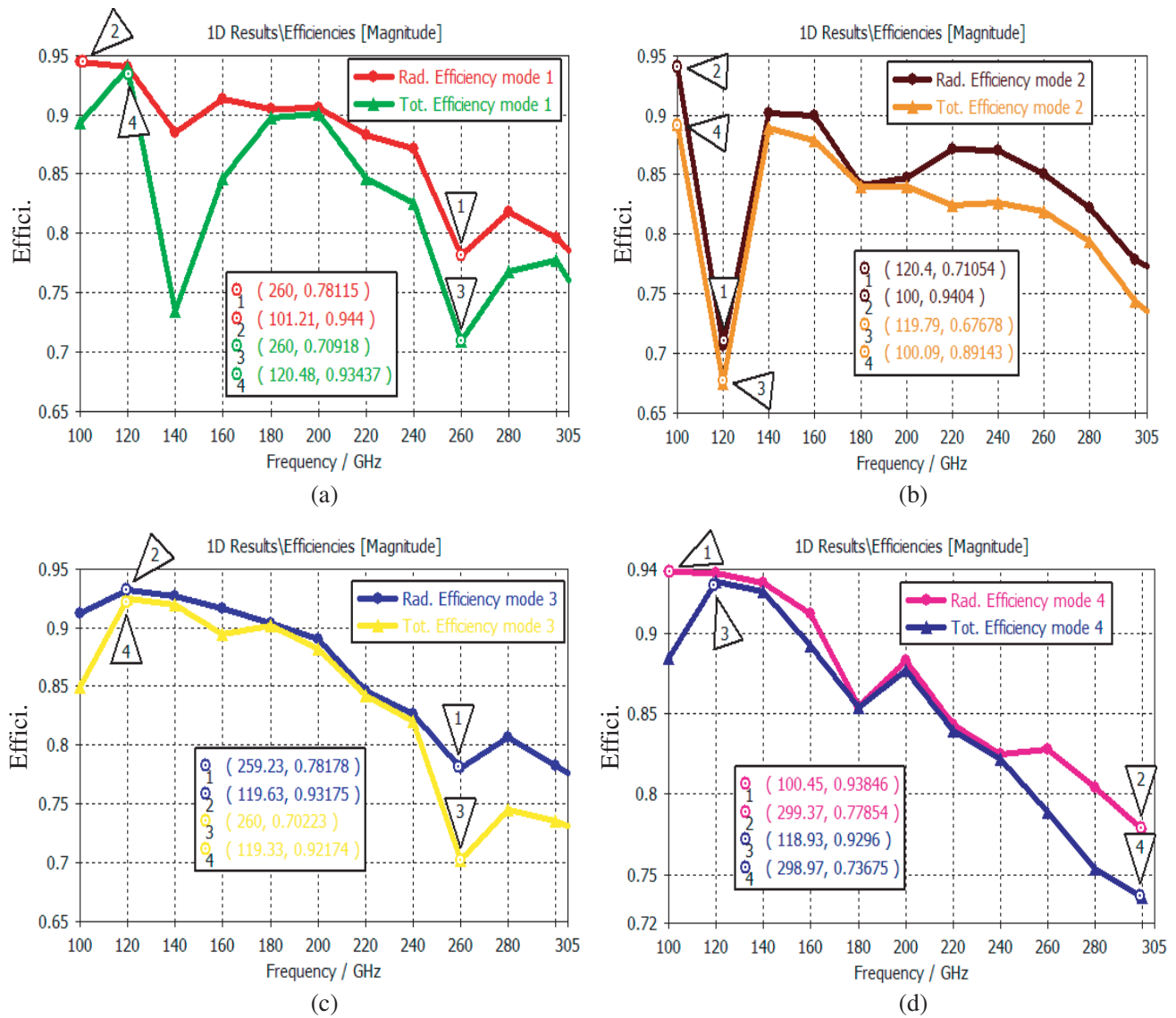
Figure 5. Simulation results of the radiation and the total efficiency of the proposed reconfigurable microstrip antenna. (a) For mode 1. (b) For mode 2. (c) For mode 3. (d) For mode 4.

the feed line, because of the skin depth effect on the alternate electric current (AC), and the surface current distribution is inversely related to the frequency, i.e., at a lower frequency, the surface current distribution is high and vice versa, and also the surface current distribution is almost independent of the PIN diodes states.

Figure 8(a) shows the simulation result comparison of S_{11} in [dB] of the proposed reconfigurable antenna, which depends on the two PIN diodes states. It has been shown that the proposed reconfigurable antenna has six different working bands, which are 100–136.88 GHz, 156.51–260 GHz, 283.91–302.85 GHz, 100–301.75 GHz, 100–260 GHz, and 100–268.16 GHz. Fig. 8(b) shows the simulation result comparison of the gain (IEEE) in (dB) when Phi = 44° of the proposed reconfigurable antenna, which depends on the PIN diodes states. It has been shown that the gain of the proposed reconfigurable antenna is between 0.17 and 8.59 dB when Phi = 44° at the frequency range of 100–300 GHz.
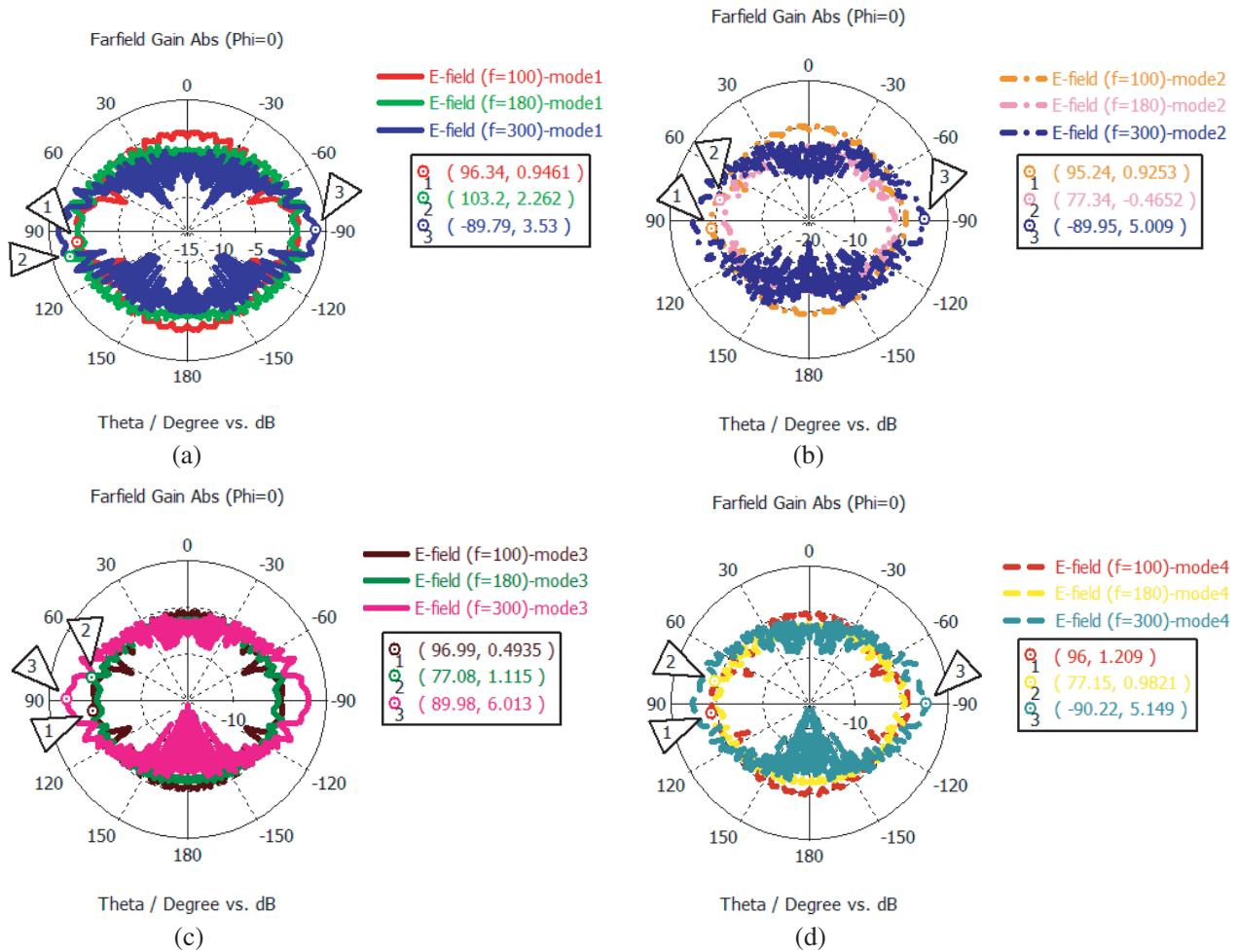
Figure 6. Simulation results of the E-field for the proposed reconfigurable microstrip antenna. (a) For mode 1. (b) For mode 2. (c) For mode 3. (d) For mode 4.

4.2. Comparison of Simulation Results of the Proposed Reconfigurable Microstrip Antenna with Declared Etching Accuracy

The following simulation results are shown in Figs. 9(a)–(d).

Figures 9(a)–(d) show the simulation results of S_{11} for the proposed reconfigurable microstrip antenna (modes 1–4) with or without etching accuracy ($\pm 5\,\mu$m), which is supposed to be when this antenna will be fabricated. This figure may show that the frequency working band may change at a frequency range about 8 GHz, when this reconfigurable antenna will be fabricated.

4.3. Comparison of Simulation Results of the Proposed Reconfigurable Microstrip Antenna

The following simulation results are shown in Fig. 10.

Figures 10(a)–(b) show the simulation results from a comparison of the gains and S_{11} in (dB) of the proposed reconfigurable antenna, which depends on the two PIN diodes states (modes 1–4), depending on the FEM and FIT solvers at the CST MWS simulator. It has been shown that a fair agreement between the simulation results is achieved regarding the proposed reconfigurable antenna, which supports the proposed antenna design.

4.4. Discussion

The objective of this research was to design and simulate, with FIT solver at the CST MWS simulator, a UWB reconfigurable microstrip antenna for the frequency range of 100–302.85 GHz with two PIN diodes, for cellular communication at mmWave/THz band for beyond 5G and comparison with the FEM solver. This microstrip antenna can change its BW, primary radiation lobes direction, or both of them with only one antenna design structure.

A mmWave/THz reconfigurable microstrip antenna is a powerful approach to realize low-profile UWB mmWave/THz antennas. To design mmWave/THz microstrip antenna, a low ε_r should be used. Moreover, low $\tan \delta$ should be used. In this research paper, BCB polymer was used, which has those
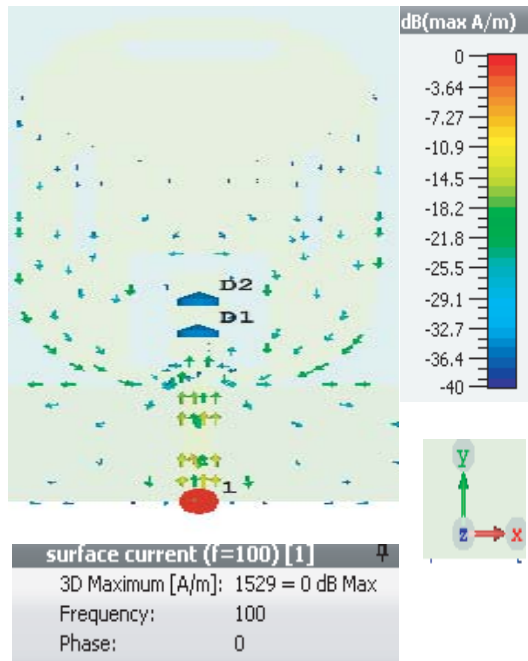
(a)
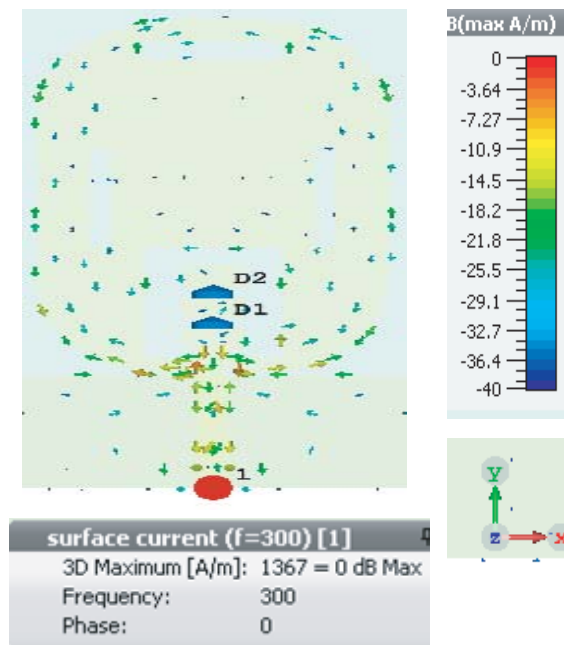
(b)
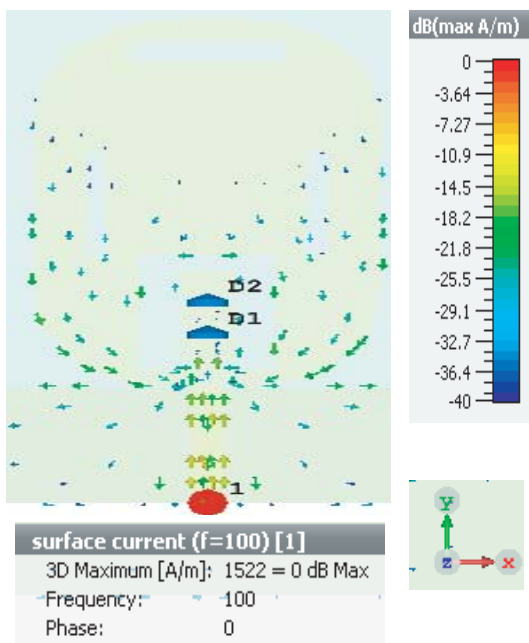
(c)
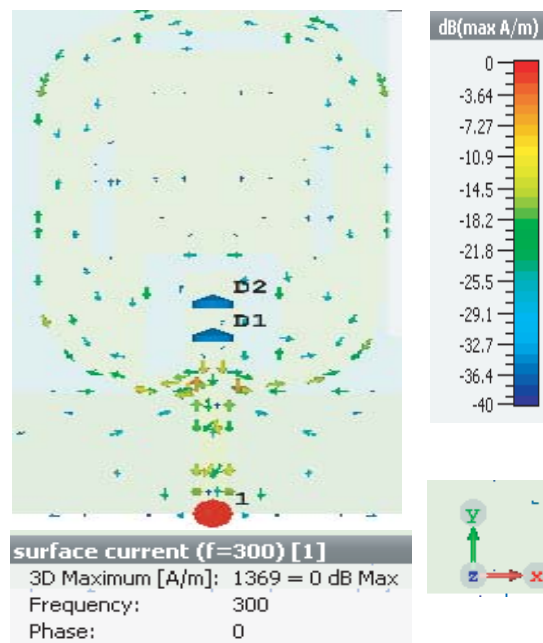
(d)
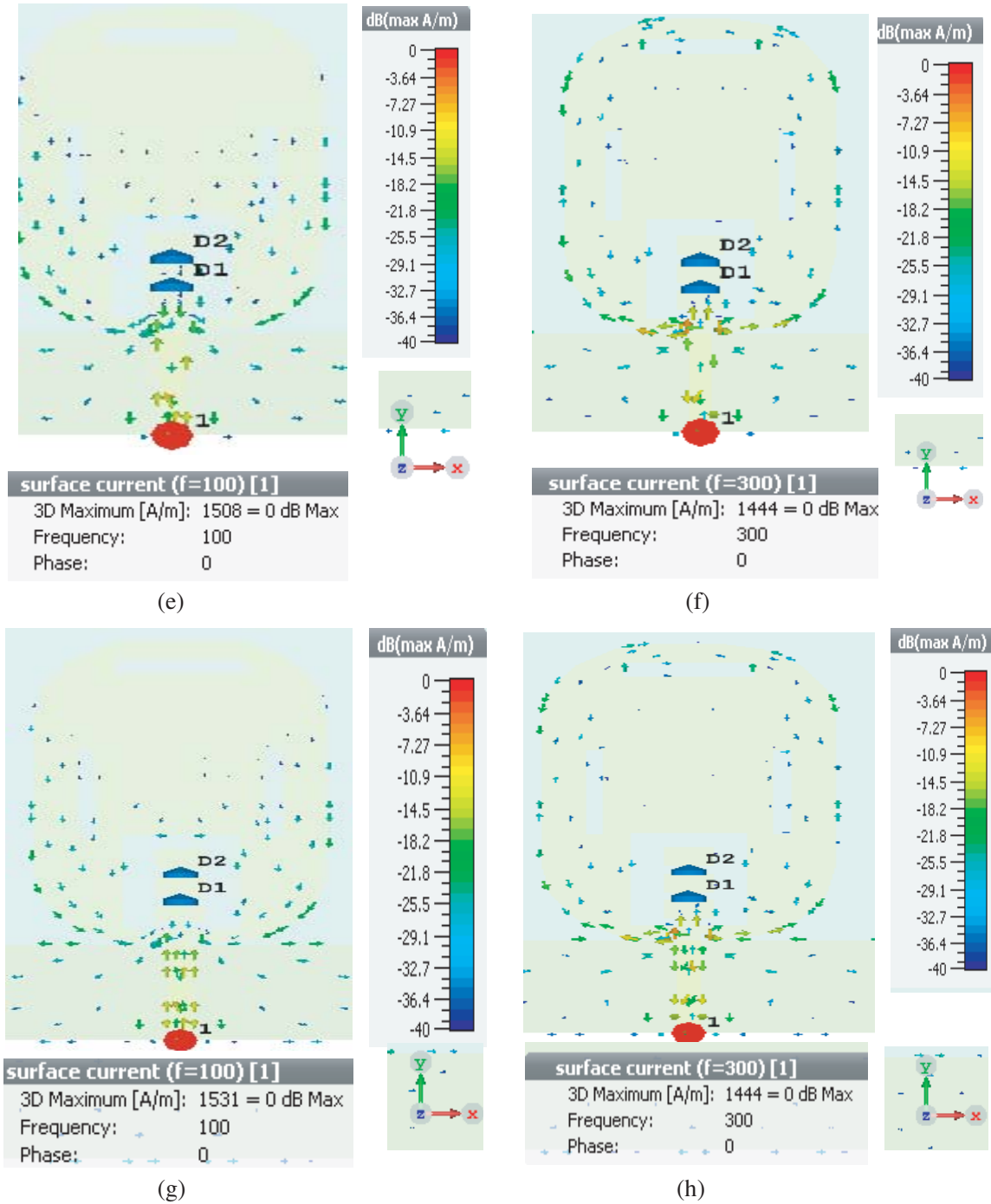
Figure 7. Simulation results of the surface current distribution of the proposed reconfigurable microstrip antenna. (a)–(b) For mode 1. (c)–(d) For mode 2. (e)–(f) For mode 3. (g)–(h) For mode 4.

features [25].

According to the simulations done with FIT solver at CST MWS simulator, the proposed antenna has six different working bands, which are 100–136.88 GHz, 156.51–260 GHz, 283.91–302.85 GHz, 100–301.75 GHz, 100–260 GHz, and 100–268.16 GHz, which depend on the two PIN diodes states, while the maximum gain and the direction of the main lobes were 8.59 dB, −90, 77, 90, 96, 97, and 103°, which depend on the PIN diodes states, respectively. The proposed antenna's simulation results were
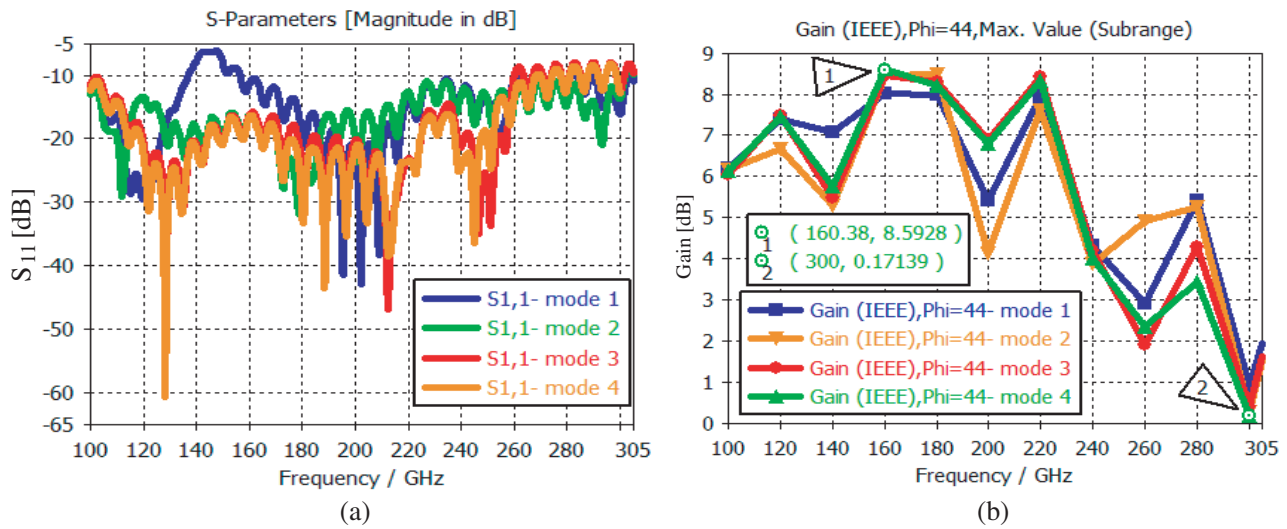
Figure 8. Comparison between the four different modes. (a) S_{11} of the proposed reconfigurable antenna. (b) Gain of the proposed reconfigurable antenna.
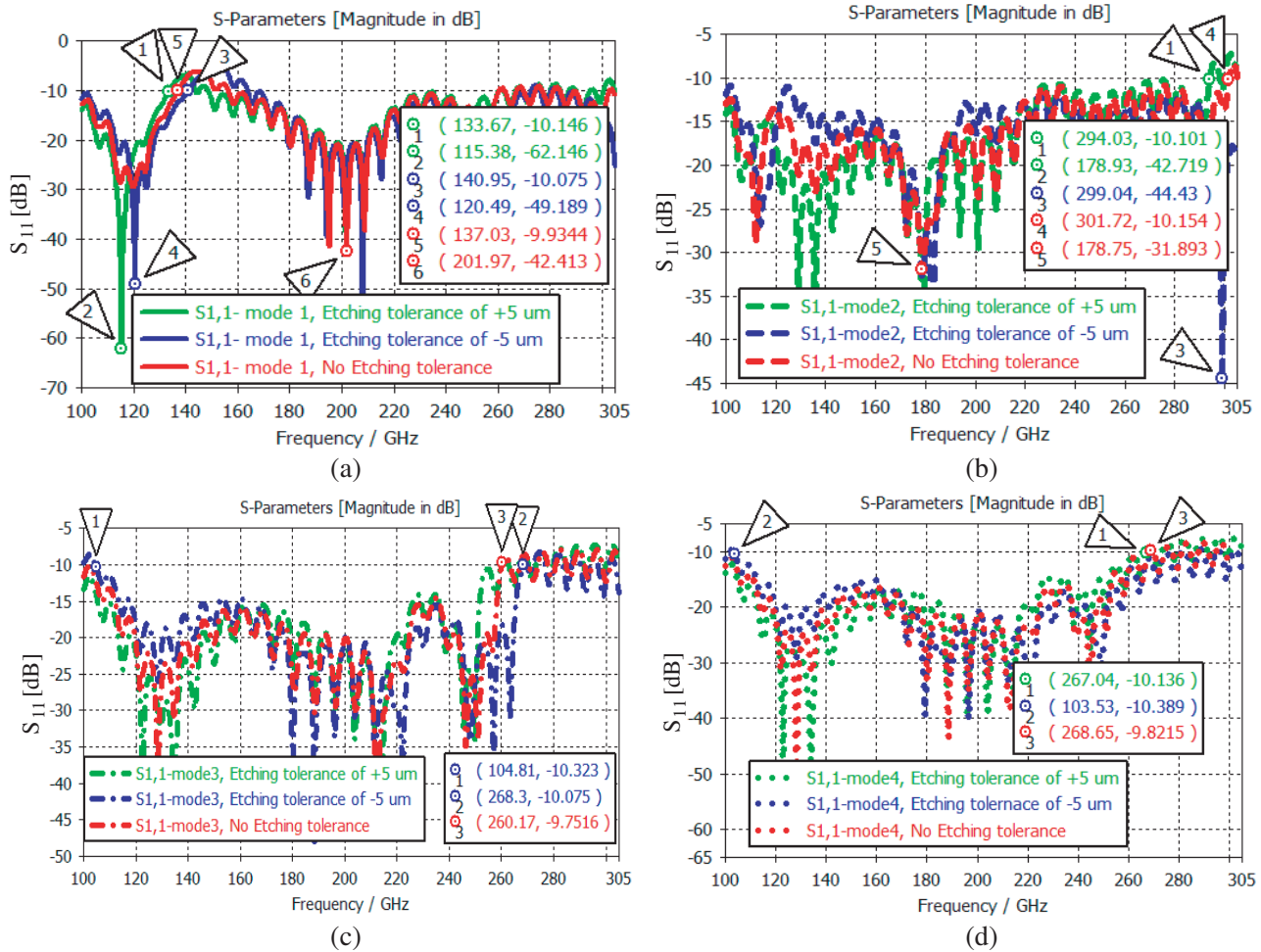
Figure 9. Simulation results of the S_{11} of the proposed reconfigurable microstrip antenna with or without the etching accuracy. (a) For mode 1. (b) For mode 2. (c) For mode 3. (d) For mode 4.
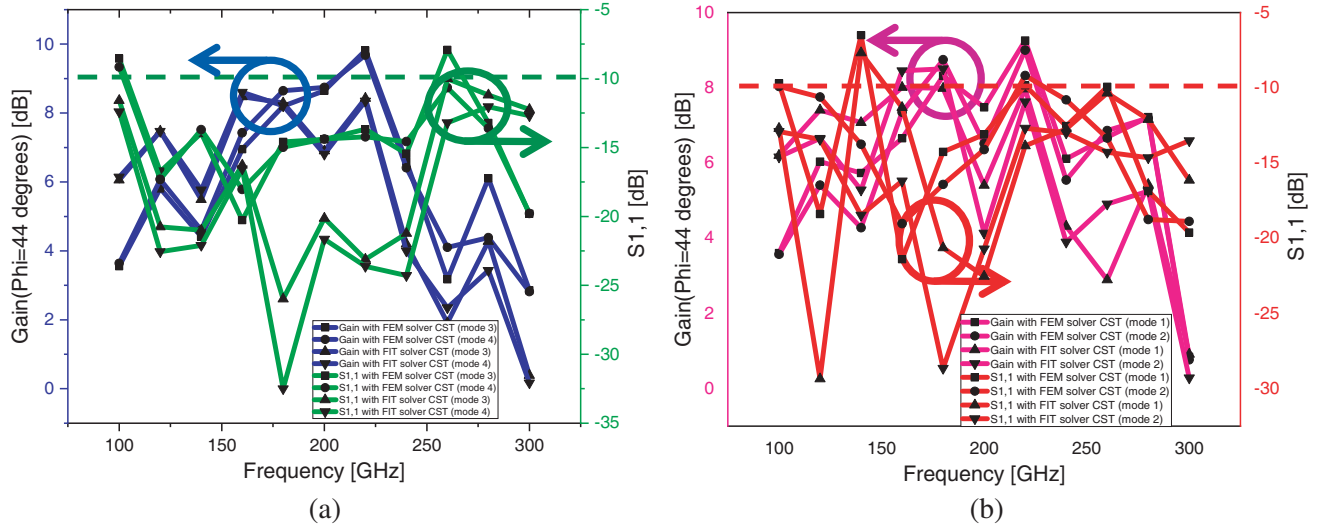
Figure 10. Comparison of the simulation results of the gain and the return loss of the proposed reconfigurable microstrip antenna. (a) For mode (1–2). (b) For mode (3–4).

Table 2. Comparison with others reported kinds of literature.

Ref.	Techno.	Reconfig. technique	Freq. nom. (GHz)	Operating frequency (GHz)	Max. directivity /gain (dBi/dB)	Main lobe angles (°)	Max. Rad. efficiency (%)
[12]	Graphene Vivaldi antenna	Electrical field bias of the graphene layer	≈ 1200	280–1400	$< 1\,dB$	n/a	n/a
	Graphene-metal Vivaldi antenna		≈ 300	210–670	$7\,dB$	n/a	n/a
[13]	Hybrid structure DRA with a graphene dipole antenna	Electrical field bias of the graphene layer	2500	1000–4000	$7\,dB$	n/a	70
[14]	Microstrip patch backing cavity with graphene/ Al_2O_3 stacks	Electrical field bias of the graphene layer	4500, 7000	4000–5000, 6500–7500	$7.2\,dBi$	-15–(25)	n/a
[15]	15×15 microstrip patch RRA antenna	Electrical-PIN diode switch	220	215–225	$21\,dBi$	0–50	43.7

Ref.	Techno.	Reconfig. technique	Freq. nom. (GHz)	Operating frequency (GHz)	Max. directivity /gain (dBi/dB)	Main lobe angles (°)	Max. Rad. efficiency (%)
[16]	Homogenous graphene substrate with dielectric grating	Electrical field bias of the graphene layer	903.9	889.325–917.455	15.89 dB /16.8 dBi	n/a	87
	PBG graphene substrate with dielectric grating		990.8	974.15–1157.3	16.39 dB /17 dBi	n/a	86.67
[17]	Pattern two element patch antenna	Electrical-2 PIN diodes switches	600	572.67–627.33	6.99 dB/7.1 dBi	−26, 26	97
[18]	Graphene antenna	Electrical field bias of the graphene layer	1780	n/a	5.8 dBi	−30, −70	n/a
[19]	Microstrip quasi-Yagi-Uda antenna with graphene	Electrical field bias of the graphene layer	≈ 500	495–510	7.5 dB	30–150	96
[20]	Concentric ring slot antenna using graphene	Electrical field bias of the graphene layer	4754–4878	4667–5073	8.6	n/a	n/a
[21]	Graphene-based metal planar microstrip antenna	Electrical field bias of the graphene layer	990–1240	≈ 805	n/a	n/a	69
This work	Microstrip patch antenna	Electrical-2 PIN diodes switches	128.2–212.25	100–302.85	8.9 dBi/8.59 dB	−90, 77, 90, 96, 97, and 103	93.4

compared by simulation with the FEM solver at the CST MWS simulator, and a fair agreement was achieved between them, supporting this design.

It may have been shown that the simulation results of this work were compared, while in works [12–21], the simulation results were not compared. Like works [12–21], the goal of this work was to design

a mmWave/THz reconfigurable antenna, but in this work, we used the PIN diodes switches to change the antenna working frequency band, like works [15, 17], while in works [12–14, 16, 18–21] the graphene layers used and by changing the electrical filed bias of the graphene layers, the researchers changed the antennas' parameters. The design and simulation were done with the CST MWS solver, like works [12–14, 16–18, 20]. In contrast, the design and simulation in work [12, 19, 21] were done with an Ansys HFSS solver.

The simulator comparison of the proposed mmWave/THz UWB reconfigurable microstrip was close, as much as can be, to experimental validation [29]. Because in the FEM and FIM solvers in the CST MWS simulator, the values of $\tan\delta$ and ε_r of the BCB polymer are measured and applied at the highest frequency @65 GHz, and these parameters are almost constant below 1500 GHz [25], while this polymer's ε_r is also constant, approximately, under ambient temperature change up to 150°C [26–28]. Furthermore, to show the possible errors of this fabrication, simulations were also performed on the possibility of this etching accuracy ($\pm 5\,\mu$m) [31], i.e., for each dimension of the antenna that has been optimized, the possible production accuracy was added/subtracted in the simulation software, and two more simulations were performed with the new values that can be after the production of the proposed antenna. Therefore, two more graphs were obtained for S_{11} which may show the S_{11} that can be obtained in prototype fabricated antenna, and the obtained results with this accuracy were relatively close to the results without this accuracy. To summarize this paragraph and the discussion, the following Table 2 is attached.

5. CONCLUSIONS

The concept of a UWB reconfigurable mmWave/THz microstrip antenna for the frequency range 100–302.85 GHz with a newfangled gold radiating patch with two PIN diodes installed on a BCB polymer is presented. The equivalent inductor (L), capacitor (C), and resistor (R) for the ON and OFF states of these PIN diodes should be 100 pH, 4 fF, and 10 ohms, respectively. These PIN diodes need to work at the frequency range of 100–303 GHz at least. These PIN diodes do not exist at the current mmWave/THz technology to our best knowledge. The reconfigurable types of the proposed antenna are frequencies, BWs, and beams reconfiguration. This reconfigurable microstrip antenna was designed and simulated with the FIT solver in the CST MWS simulator, while the comparison was with the FEM solver in the CST MWS simulator. The simulation results obtained from the two solvers were in a fair agreement, supporting the proposed antenna design. Furthermore, the simulation results of the maximum gain, BW, and total efficiency obtained for the proposed antenna were 8.59 dB, > 201.77 GHz ($> 100.44\%$), and 93.4%, respectively. These antennas may be used for cellular communication at mmWave/THz band beyond 5G.

REFERENCES

1. Jha, K. R. and G. Singh, *Terahertz Planar Antennas for Next Generation Communication*, Springer International Publishing Switzerland, 2014.
2. Tekbiyik, K., A. R. Ekti, G. K. Kurt, and A. Gorcin, "Terahertz band communication systems: Challenges, novelties and standardization efforts," *ELSEVIER Physical Communication*, Vol. 35, 100700, 1–18, May 2019.
3. Akyildiz, I. F., C. Han, and S. Nie, "Combating the distance problem in the millimeter-wave and terahertz frequency bands," *IEEE Communications Magazine*, Vol. 56, No. 6, 102–108, June 2018.
4. Han, C. and Y. Chen, "Propagation modeling for wireless communications in the terahertz band," *IEEE Communications Magazine*, Vol. 56, No. 6, 96–101, June 2018.
5. Schneider, T., A. Wiatrek, S. Preobler, M. Grigat, and R. P. Braun, "Link budget analysis for terahertz fixed wireless links," *IEEE Transactions on Terahertz Science and Technology*, Vol. 2, No. 2, 250–256, March 2012.
6. Zhao, J., "A survey of reconfigurable intelligent surfaces: Towards 6G wireless communication networks with massive MIMO 2.0," *arXiv:1907.04789*, 1–7, July 2019.

7. Luo, Y., Q. Zeng, X. Yan, T. Jiang, R. Yang, J. Wang, Y. Wu, Q. Lu, and X. Zhang, "A graphene-based tunable negative refractive index metamaterial and its application in dynamic beam-tilting terahertz antenna," *WILEY Periodicals Microwave and Optical Technology Letters*, Vol. 61, No. 12, 2266–2672, December 2019.

8. Bansal, G., A. Marwaha, and A. Singh, "A graphene-based multiband antipodal Vivaldi nanoantenna for UWB applications," *Springer Nature Journal of Computational Electronics 19*, 709–718, February 2020.

9. Wang, C. L., Y. Q. Wang, H. Hu, D. J. Liu, D. L. Gao, and L. Gao, "Reconfigurable sensor and nanoantenna by graphene-tuned Fano resonance," *OSA Optics Express*, Vol. 27, No. 24/25, 35925–35935, November 2019.

10. Chen, Z. N., *Handbook of Antenna Technologies*, Springer Science, September 2016.

11. Christodoulou, C. G., Y. Tawk, S. A. Lane, and S. R. Erwin, "Reconfigurable antennas for wireless and space applications," *Proceedings of the IEEE*, Vol. 100, No. 7, 2250–2261, July 2012.

12. Jin, J., Z. Cheng, J. Chen, T. Zhou, C. Wu, and C. Xu, "Reconfigurable terahertz Vivaldi antenna based on hybrid graphene-metal structure," *WILEY RF and Microwave Computer-Aided Engineering*, 1–8, January 2020.

13. Hosseininejad, S. E., M. Neshat, R. Faraji-Dana, S. Abadal, M. C. Lemme, P. H. Bolivar, E. Alarcon, and A. Cabellos-Aparicio, "Terahertz dielectric resonator antenna coupled to graphene plasmonic dipole," *IET 12th European Conference on Antennas and Propagation (EuCAP 2018)*, 1–5, 2018.

14. Dong, Y., P. Liu, D. Yu, G. Li, and F. Tao, "Dualband reconfigurable terahertz patch antenna with graphene-stack-based backing cavity," *IEEE Antennas and Wireless Propagation Letters*, Vol. 15, 1541–1544, February 2016.

15. Sun, L., B. Li, M. Wu, and X. Lv, "A 1-bit 220 GHz reconfigurable reflectarray," *IEEE 2019 International Conference on Microwave and Millimeter Wave Technology (ICMMT 2019)*, 1–2, Guangzhou, China, May 19–22, 2019.

16. Kushwaha, R. K. and P. Karuppanan, "Parasitic-coupled high-gain graphene antenna employed on PBG dielectric grating substrate for THz applications," *WILEY Microwave Optical Technology Letter*, 1–9, 2019.

17. Usman, M., S. Tanoli, F. Khan, W.-U.-R. Khan, S. M. Umar, and S. Ullah, "Pattern reconfigurable two element printed patch antenna for THz wireless applications," *IEEE 2020 3rd International Conference on Computing, Mathematics and Engineering Technologies (iCoMET2020)*, 1–7, Sukkur, Pakistan, January 29–30, 2020.

18. Varshney, G., "Reconfigurable graphene antenna for THz applications: A mode conversion approach," *IOP Publishing Nanotechnology*, Vol. 31, No. 13, 1–16, January 2020.

19. Yao, W.-L., X.-G. Guo, Y.-M. Zhu, and P. Li, "Terahertz beam reconfigurable micro-strip Quasi-Yagi-Uda antenna based on monolayer graphene," *Springer Journal of Infrared, Millimeter, and Terahertz Waves*, Vol. 39, No. 1, 39–46, February 2020.

20. Krid, H. B., Z. Houaneb, and H. Zairi, "Reconfigurable graphene annular ring antenna for medical and imaging applications," *Progress In Electromagnetics Research M*, Vol. 89, 53–62, 2020.

21. Dash, S. and A. Patnaik, "Behavior of graphene-based planar antenna at microwave and terahertz frequency," *ELSEVIER Photonics, and Nanostructures — Fundamentals and Applications*, Vol. 40, 1–13, April 2020.

22. Parchin, N. O., H. J. Basherlou, Y. I. A. Al-Yasir, A. M. Abdulkhaleq, and R. A. Abd-Alhameed, "Reconfigurable antennas: Switching techniques — A survey," *IMDP Electronics*, Vol. 9, No. 36, 1–14, May 2020.

23. Tanaka, Y., H. Uda, H. Hayashi, H. Ueda, and M. Usui, "A 76–77 GHz high isolation GaAs PIN-diode switch MMIC," *R&D Review of Toyota CRDL*, Vol. 37, No. 2, 19–26, May 2002.

24. Bondarik, A. and D. Sjöberg, "Pattern reconfigurable wideband stacked microstrip patch antenna for 60 GHz," *Springer International Journal of Antennas and Propagation*, 1–12, May 2016.

25. Borgia, A., "New materials and technologies for compact antennas and circuits at millimeter frequency," Ph.D. thesis, Electrical and Electronics Engineer, 2010.

26. Woehrmann, M. and M. Toepper, "Polymerization of thin film polymers," *INTECH Open Science*, 113–138, Sep. 2012.

27. Su, T., W. Men, Z. Wang, L. Xuan, and W. Zhao, "POSS-benzocyclobutene (POSS-BCB) resin: A hybrid thermosetting material with high thermal stability and a lowdielectric constant," *SAGE High-Performance Polymers*, 1–7, November 2017.

28. Huang, C., L. Pan, R. Liu, and Z. Wang, "Thermal and electrical properties of BCB-liner through-silicon vias," *IEEE Transactions on Components, Packaging and Manufacturing Technology*, Vol. 4, No. 12, 1936–1946, December 2014.

29. U. Nissanov (Nissan), G. Singh, E. Gelbart, and N. Kumar, "Highly directive microstrip array antenna with FSS for future generation cellular communication at THz band," *Springer Nature Wireless Personal Communications*, 1–20, January 2021.

30. https://www.3ds.com/products-services/simulia/products/cst-studio-suite.

31. http://www.pcb-tecnomec.com.